This article has been accepted for publication in IEEE Transactions on Power Delivery. This is the author's version which has not been fully edited and content may change prior to final publication. Citation information: DOI 10.1109/TPWRD.2024.3453270

Perturbation-Based Load Sensitivity Identification for Solid-State Transformer-Based Load Control

Maëva Courcelle, *Student Member, IEEE*, Qiucen Tao, *Student Member, IEEE*, Johanna Geis-Schroer, *Student Member, IEEE*, Thomas Leibfried, *Senior Member, IEEE*, and Giovanni De Carne, *Senior Member, IEEE*

***Abstract*—In recent years, the electricity supply has become more volatile, and advanced real-time controllers are needed to manage the grid safely. Demand-side management represents a promising solution, where regulating load consumption through controlled voltage variations offers a valuable approach, which can be applied using power electronics actuators. This approach relies on understanding how power consumption reacts to changes in voltage magnitude or frequency. One proposed method is perturbation-based load sensitivity identification, which introduces controlled perturbation into the grid, for instance through a Solid-State Transformer, and calculates load parameters via power measurements. However, existing methods often require synchronization with the perturbation actuator and lack resiliency to noise or uncorrelated power variations, limiting their practical applicability. This paper proposes a novel approach for perturbation-based load sensitivity identification, utilizing a pre- and post-filtering process. This method has been tested under realistic grid conditions, with autonomous computation of the load sensitivity, triggered by variation-based perturbation detection. It offers more global and flexible control possibilities, and eliminates the need for complex communication layers.**

***Index Terms*—Solid-State Transformer, Load sensitivity, Demand-side management, Microgrids, Power control.**

I. Introduction

THE energy system is moving toward a high penetration of power electronics-based and intermittent energy sources such as photovoltaic and loads, e.g., electric vehicles. As a consequence, the electricity supply becomes less predictable, and advanced real-time controllers are needed to manage the grid operations within the operational limits. A potential solution is the smart load control, wherein grid operators adjust not only generation but also consumption to align with the supply [1], [2]. However, this approach faces hurdles like limited communication infrastructure and privacy concerns related to user information [3]–[5].

As an alternative solution, Conservation Voltage Reduction (CVR) influences load consumption by changing the voltage ratio in transformers by means of on-load tap-changers [6]–[8]. Although effective, CVR operates with slow dynamics (depending on the tap-changer technology) and coarse granularity. In contrast, Solid-State Transformer (SST) offers finer granularity and faster dynamic characteristics for active and reactive power modulation [9]. The SST, working as a grid-forming unit, can dynamically adjust voltage waveform characteristics enabling a voltage (or frequency)-based load control [10]–[12].

However, enhanced control actions can be achieved with accurate knowledge of the load sensitivity to voltage and frequency, wherein the load sensitivity represents the percentage of power change resulting from a change in voltage characteristics. Two common models for estimating the load sensitivity are the polynomial model (ZIP model) [13] and the exponential model [14]. This paper adopts the exponential load model due to its simplicity and straightforward interpretation for future control [15]. The load model parameters are evaluated by means of a measurement-based approach involving fitting algorithms to quantify active and reactive power variations resulting from voltage or frequency changes [16], [17]. These changes can be either natural such as tap-changer adjustments [18], [19], or triggered perturbations (introduced by Solid-State Transformer (SST) [20], [21]). Our approach employs an actuator capable of generating disturbances, as represented by the AC/AC converter in Fig. 1. Measurement devices analyze recorded voltage and power during these disturbances to calculate the load sensitivity. When measurement devices are strategically positioned at different locations, the load sensitivity can be assessed across multiple nodes. Most of the works use a voltage threshold to detect the voltage perturbations. However, a fixed threshold may not be applicable for different measurement points, especially in case of voltage drop along electrical lines. This limitation makes global control challenging, as no information about the load sensitivity across connected nodes would be available. Furthermore, only a few published works consider power variations influenced by external factors (human behavior, intrinsic load behavior), which often invalidate simple voltage-power correlations [22], [23].

This study introduces a perturbation-based load sensitivity algorithm designed for real-world scenarios. Unlike existing methods limited by their dependency on precise synchronization and their inability to handle noise and unintended power changes effectively, our approach detects the disturbance and analyzes the correlation of voltage and power. Moreover, experimental validation is conducted in the *Energy Smart Home Lab* at the *Karlsruhe Institute of Technology*, accurately reproducing daily load scenarios while offering testing flexibility.

With respect to the existing literature (see Table I), key contributions of this work include:

- A disturbance detection method based on variation crite-

This work has been supported by the Helmholtz Association under the program "Energy System Design" and under the Helmholtz Young Investigator Group "Hybrid Networks" (VH-NG-1613).

ria, eliminating the need for synchronization with main actuators and consequently time delay issues.
- Reliable load sensitivity calculation, resilient to noise and unintended power changes via pre- and post-processing filtering, ensuring good performance in unpredictable real-world scenarios.
- Realistic experimental validation in household conditions, offering a higher degree of realism and flexibility in testing, which was missing in field measurements and simulations.

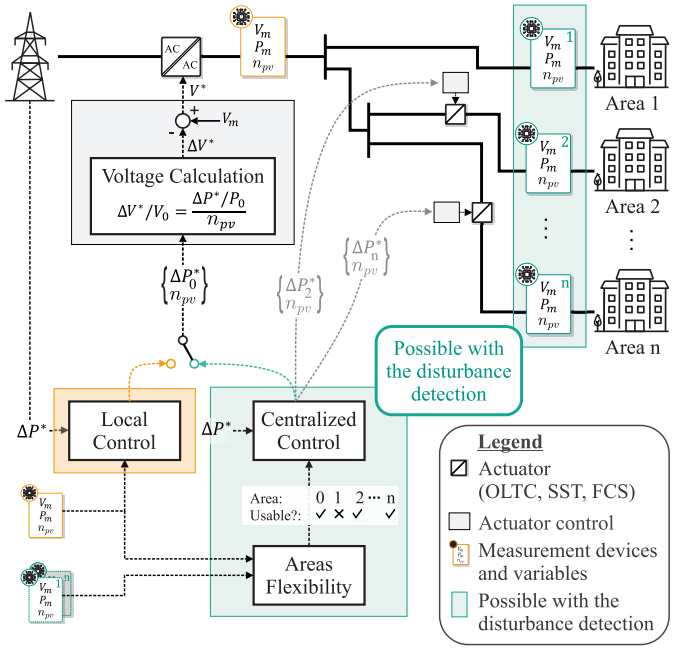

Fig. 1: Examples of voltage-based power controls, where the load sensitivities are used for the actuator's voltage set-point calculation, showing the unlocked flexibility offered by the proposed disturbance detection method.

In summary, this paper presents an approach to estimate load sensitivity through a perturbation-based algorithm suitable for real-world application. The experimental validation not only showcases its effectiveness but also demonstrates its practical applicability. The work is structured as follows: Section II elucidates voltage-based load control using Solid-State Transformers and outlines the methodology for perturbation-based load parameter calculation. Section III provides a comprehensive background on load sensitivity identification. Section IV delves into the algorithm and presents simulation results. Real-world load sensitivity computation outcomes are showcased in Section V. Finally, the conclusions are drawn in Section VI.

II. Solid-State Transformer-based Load Control

The efficacy of voltage-based load management has been substantiated by its successful implementation in initiatives like CVR [7], [36] and the CLASS project [12]. A pivotal element within this framework is the online tap-changer (OLTC), responsible for regulating the voltage amplitude within the low-voltage (LV) grid. This investigation has paved the way for the emergence of an alternative actuator, known as the Solid-State Transformer (SST). Functioning as a power electronic-based AC/AC converter, the SST presents, among various advantages, a heightened capability for precise voltage amplitude regulation [37].

The SST aims to replace the conventional transformers and to provide ancillary services, like power quality improvement, EV charging station integration, or soft load reduction [38], also including the ability to interface with DC microgrids. Although the SST is not yet commercialized, much work has been done on its topology design and efficiency, which has already been experimentally proven with prototypes [39], [40].

The SST typically has a 3-stage converter configuration [38]. This configuration involves a medium voltage (MV) converter balancing the MV DC link voltage, the DC/DC converters transforming the voltage from MV to LV, and the LV converter grid-forming the LV voltage under specific voltage waveform set-points (e.g. amplitude, frequency or phase) [41].

As demonstrated in the literature [10], [42]–[44], voltage amplitude and frequency variations can be used to influence the load consumption in an active way, enabling a new approach to obtain power flexibility. However, it must be noted that its control accuracy is highly dependent on the load sensitivities and their estimation approaches. Indeed, the sensitivities' values are used as a reference to calculate the effect of the voltage variation on the power consumption [10], allowing the actuator to apply a precise load reduction when required. As shown in the grey control area of Fig. 1, the SST voltage set-point V^* is calculated based on the required power variation ΔP^* and the load sensitivity n_{pv}. This set-point provided for the load control is based on three steps:

- *LV side measurements*: Voltage amplitude and power are measured during a disturbance.
- *Load sensitivity estimation*: The load sensitivity parameter is calculated from the measured power and voltage amplitude.
- *Voltage set-point calculation*: The voltage set-point, fed to the SST controller, is given by (1), which is based on the power set-point and the load sensitivity value.

$$\Delta V^*/V_0 = \frac{\Delta P^*/P_0}{n_{pv}} \tag{1}$$

where V^* is the output voltage set-point, ΔP^* is the input power set-point, n_{pv} is the load sensitivity, and V_0 and P_0 are the rated voltage and power.

Remark: The SST is presented here as an example of an actuator providing ancillary services [45]. In fact, some works are already using the load sensitivity in various applications and actuators types, such as CVR [8], frequency support for asynchronous grid [43], [44], frequency support through HVDC-based load control [46], [47], load-control approach in MV grid with Fast Charging Stations [48], [49], or voltage-led control [11], [12]. We also highlight that the method can detect voltage amplitude disturbances as well as frequency disturbances at any node, as both voltage amplitude and frequency can be set by an SST unit.

TABLE I: Existing works on load parameter calculation and disturbance detection.

Event	Required disturbance shape (voltage amplitude)	Disturbance repeatability[a]	Disturbance detection criteria *	Uncorrelated power changes filtered	Computational autonomy and flexibility of the detection[b]	Online experimental validation	Focus of the work	References
Natural event (incl. tap change)	Variations (any kind)	/	$\begin{cases}\text{corr}(V,P)>0\\ \Delta FT>Th\end{cases}$	✓	+ +	✗	Machine learning-based steady-state ZIP parameters and load sensitivity estimation	[24], [25], [22]
		/	$\lvert\mathcal{M}(V)\rvert\neq 0$	✓	+ +	✗	Time-varying ZIP parameters calculation for CVR	[26], [27], [23]
		- -	$\begin{array}{l}\Delta V>Th\\ \Delta I>Th\\ n_{pv}>Th\end{array}$	✗	+	✗	Event filtering for load modeling	[28]
		- -	$\begin{cases}\Delta V_{t_k}>Th\\ \Delta V_{t_{k+1}}>Th\end{cases}$	✗	- -	✗	Hybrid state estimation and load modeling	[29]
		- -	$\begin{cases}\Delta V>Th\\ n_{pv}>Th\\ \Delta P/\Delta V>0\end{cases}$	✗	-	✗	Load modeling for CVR	[30]
	Step	- -	$\Delta V>Th$	✗	-	✗	Statistical load modeling	[31]
		- -	$\Delta V>Th$	✗	-	✗	Load modeling	[32]
On-demand tap change	Step	-	$\begin{cases}\Delta V>Th\\ \Delta P/\Delta V>0\end{cases}$	✗	-	✗	Effet of events on load modeling	[18]
		-	$\Delta V>Th$	✗	-	✗	Load modeling	[33], [34]
On-demand SST-based disturbance	Ramp	+	Synchronization signal	✗	- -	✓	Load modeling for voltage-based load control	[10], [20], [21]
		+	Synchronization signal	✗	- -	✗	Load modeling for voltage-based load control	[35]
	Variations Paper: Sinus Tested: Step, Ramp, Triangular	+ +	$\begin{cases}\sigma(V)>Th\\ \sigma(P)<Th\\ \Delta\sigma(P)<Th\\ n_{pv}>Th\end{cases}$	✓	+ +	✓	Load modeling for voltage-based load control	**This paper**

*** Notations** corr(V,P): correlation matrix; Th: threshold; FT: features matrix; $\lvert\mathcal{M}(V)\rvert$: determinant of the voltage measurements matrix

[a] Disturbance repeatability indicates how often a disturbance can be replicated in a system.

[b] Computational autonomy and flexibility of the detection refers to the ability to operate without human intervention and adapt to various disturbances.

[a] and [b]: ++ : High, + : Moderate, - : Low, - - : Very low

III. Load Sensitivity Identification

In order to assess the load sensitivity, the exponential load model with frequency dependency has been chosen in this work [17]. This model was selected for its simplicity and coherence for voltage-based control purposes. Unlike the ZIP model, which requires estimating at least two independent variables, the exponential model involves only one variable per equation. Moreover, the exponent directly reflects the sensitivity of power to voltage changes [14], [15].

It is well known that load model parameters vary with time as the load consumption is constantly evolving due to factors such as human interaction, weather conditions, or internal load behavior [26]. To avoid overloading the notation, the time variable is omitted, and the exponential load model with frequency dependency can be written as follows:

$$P = P_0 \cdot (\frac{V}{V_0})^{n_{pv}} \cdot (\frac{f}{f_0})^{n_{pf}} \tag{2}$$

$$Q = Q_0 \cdot (\frac{V}{V_0})^{n_{qv}} \cdot (\frac{f}{f_0})^{n_{qf}} \tag{3}$$

where V is the RMS voltage, f is the current frequency, V_0 and f_0 are the rated voltage and frequency respectively, P_0 and Q_0 are the active and reactive power taken at V_0 and f_0, and n_{pv}, n_{qv}, n_{pf}, n_{qf} describe active and reactive power-to-voltage and frequency sensitivities respectively, which are ratios and therefore dimensionless quantities.

A. Perturbation-Based Load Sensitivity Identification

The measurement-driven technique computes load parameters by analyzing power measurements within the grid. The data is refined to identify a pertinent time interval,

such as when a voltage fluctuation has occurred, leading to a discernible change in power [18]. More recently, an extension of the measurement-based method, the perturbation-based method, avoids this post-data processing and has been proposed in [20]. In this method, a small artificial amplitude or frequency variation of the voltage is applied to a part of the grid by means of an actuator, such as an SST. Using intentional perturbations, the load sensitivity calculation window is actually the perturbation window known to the actuator. The load sensitivity can then be calculated in real time from the measurements. Since SST can emulate any perturbation [44], in this work, it is decided to emulate sinusoidal variations in voltage amplitude or frequency.

The load power is always a function of voltage and frequency. However, for studies, the power sensitivity to voltage and frequency are usually decoupled: either a voltage or a frequency perturbation is introduced, and the second variable (voltage or frequency) is kept constant during the perturbation. Thus, the power sensitivity-to-voltage is calculated for a constant frequency, while the power-to-frequency sensitivity is calculated for a constant voltage. This assumption can be considered generally valid for two reasons: it is rare for both variations to occur naturally at the same time; and if they are intentional (e.g., with a tap-changer or a SST), they can be controlled to remain constant.

In this work, a sinusoidal disturbance signal of 0.8 Hz is applied every 15 s for a duration of 5 s. This perturbation is applied on the voltage, where the nominal magnitude is V_0=230 V and the nominal frequency f_0=50 Hz. In order to comply with the European grid standards, the perturbation amplitudes remain in the following ranges: $\Delta f \in [\pm 0.1\,\text{Hz}; \pm 1\,\text{Hz}]$ and $\Delta V \in [\pm 1\%; \pm 5\%]$ of V_0. The load parameter values are then calculated during the perturbation, as described in the following section, and averaged to build the load sensitivity.

B. Load Sensitivity Calculation

This section presents the basics of load sensitivity identification, as introduced in [20]. This method consists of generating a disturbance in voltage magnitude or frequency and recording the active and reactive power. From the measured voltage, frequency, and power, the load sensitivities are calculated using the method explained in this section.

1) Sensitivity to voltage: In case of the exponential model, the power-to-voltage sensitivity n_{pv} can be calculated as follows:

$$n_{pv} = \left.\frac{\mathrm{d}P/P_i}{\mathrm{d}V/V_i}\right|_{V=V_i} \tag{4}$$

where the normalization point V_i can be chosen arbitrarily, and $P_i = P|_{V=V_i}$.
Following the theory in [20], (4) can be rewritten as:

$$n_{pv} = \frac{(P_k - P_{k-1})/P_{k-1}}{(V_k - V_{k-1})/V_{k-1}} \tag{5}$$

where P_k and V_k are power and voltage at current time step t_k. The reactive power-to-voltage sensitivity n_{qv} can be calculated in the same way.

2) Sensitivity to frequency: Similarly to the voltage sensitivity, the power-to-frequency sensitivity can be expressed as:

$$n_{pf} = \left.\frac{\mathrm{d}P/P_i}{\mathrm{d}f/f_i}\right|_{f=f_i} \tag{6}$$

where the normalization point f_i can be chosen arbitrarily, and $P_i = P|_{f=f_i}$.
The sampled n_{pf} can be written as:

$$n_{pf} = \frac{(P_k - P_{k-1})/P_{k-1}}{(f_k - f_{k-1})/f_{k-1}} \tag{7}$$

where P_k and f_k are power and frequency at current time step t_k. The sensitivity calculation approach using (7) are presented in Fig. 2.

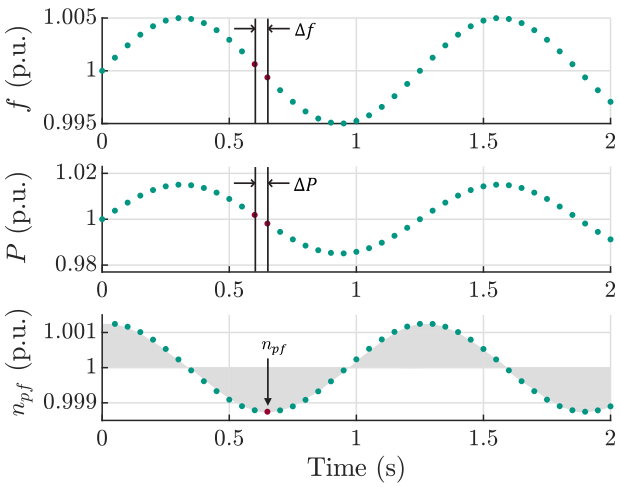

Fig. 2: Load sensitivity calculation error for an ideal frequency disturbance of ±0.5 % and an ideal power waveform with n_{pf} normalized at $n_{pf\,0} = 3$.

C. Systematical Calculation Error

The load sensitivity calculation using (5) and (7) are based on the linearization of the load model. This can lead to calculation errors depending on several parameters such as the disturbance amplitude, the base load sensitivity, or the measurement sampling time [35]. These errors are quantified here by simulation. Two types of error are considered: the error computed after averaging over a perturbation interval and the maximum deviation from the correct value. Both of them are relative errors, normalized at the base sensitivity value $n_{pv\,0}$. They represent the percentage deviation from the base value, where $n_{pv\cdot\text{raw}}$ are the raw calculations of the load sensitivity during the disturbance time window and $n_{pv\cdot\text{Avg}}$ is the average of $n_{pv\cdot\text{raw}}$ during the disturbance.

1) Error after averaging: The error after averaging represents the deviation of the calculated sensitivity from the base sensitivity. The calculated sensitivity is the average of all sensitivities calculated during the disturbance time window.

$n_{pv\cdot\mathrm{Avg}}$ is the estimate of the base value by averaging, and its estimation error can be written as follows:

$$Err_{\mathrm{Avg}} = \frac{n_{pv\cdot\mathrm{Avg}} - n_{pv\,0}}{n_{pv\,0}} \tag{8}$$

2) Maximum deviation error: The maximum deviation error is the maximum difference between the raw sensitivity calculated during the disturbance and the base sensitivity. This gap has a direct effect on the average sensitivity, especially in the case of asymmetric results (different deviations for over- and underestimated sensitivities). The maximum deviation can be expressed as follows:

$$Err_{\mathrm{max}} = \frac{\max(n_{pv\cdot\mathrm{raw}} - n_{pv\,0})}{n_{pv\,0}} \tag{9}$$

The calculation error can be seen in Fig. 2, where two successive measurements of frequency and power are used as in (7) to calculate the load sensitivity (the power-to-frequency sensitivity in this case). In the graphs, f, P and n_{pf} are normalized at f_0, P_0 and $n_{pf\,0}$ to make the calculation error more intuitive. The selected red point on the load sensitivity graph shows the location of the largest calculation error for a frequency disturbance of 0.5 % and a base sensitivity of $n_{pf\,0} = 3$. The grey area actually shows that the load sensitivity calculation based on (5) or (7) always introduces a calculation error.

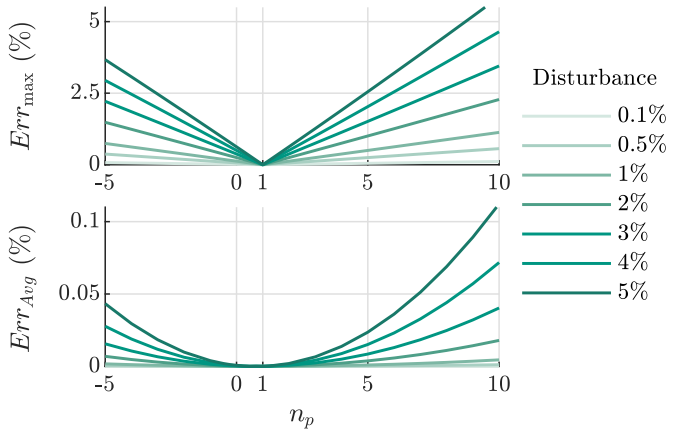

Fig. 3: Load sensitivity identification error for different disturbance amplitudes and load sensitivities.

In fact, the calculation error depends on several parameters, including the actual load sensitivity and the disturbance amplitude. The influence of these two parameters can be seen in Fig. 3. The figure shows the maximum calculation error of (9) and the error after averaging of (8) for different base load sensitivities (x-axis) and different perturbation amplitudes (color variation). The load sensitivity range $[-5; 10]$ has been chosen according to some previous results found in the literature [50], [51]. The computational error comes from the linearization of the load model, which leads to the fact that a load sensitivity of $n_p = 1$ makes the load model linear. Therefore, the approximation of (5) becomes a real slope calculation without any error. Thus, the identification accuracy depends on the actual load sensitivity value and amplitude of the disturbance, where the error can be significantly reduced by averaging the calculated sensitivity over the disturbance time window.

IV. Implementation of the Disturbance Detection for Load Sensitivity Calculation

Previous section has highlighted that the load sensitivity calculation introduces a systematic error, which can be significantly reduced by averaging the calculated values over an entire number of disturbance periods. Previous works [10], [35] used a synchronization signal, coming from the actuator itself (real-time simulator), while this work has created a mathematical tool able to detect the start and end of the disturbance without external synchronization. The disturbance detection and data processing after the load sensitivity calculation are shown in Fig. 4 and described in the following sections.

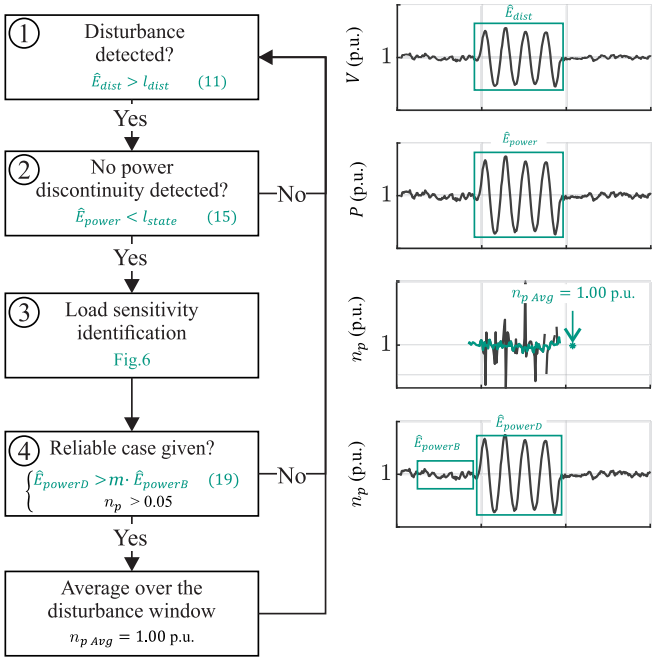

Fig. 4: Perturbation detection and data processing for real applications of load sensitivity identification.

As already mentioned in Section III-A, the load sensitivity calculation takes place during a voltage (or frequency) disturbance. In this work, the perturbation is a sinusoidal change in voltage amplitude or in frequency. The disturbance parameters are fixed for the demonstration, but the detection works for different disturbance frequencies and lengths.

① *Disturbance detection*

The detection consists of comparing the voltage (or frequency) variation with a defined limit l_{dist}.

This section describes the detection of the perturbation using only voltage measurements without any external synchronization signal. The detection of a disturbance in frequency is equivalent to the detection of a disturbance in voltage amplitude.

i) Definition of $\hat{E}_{dist}$: To detect a perturbation, this work uses a created estimator, which quantifies the voltage amplitude variation. The normalized standard deviation σ_N is first considered, which is calculated over N points. The idea of the detection is to create an estimator based on the standard deviation, where the estimator values are higher than a defined limit l_{dist} when a perturbation occurs. The estimator of voltage variation $\hat{E}_{dist}$ is defined as:

$$\hat{E}_{dist} = \frac{\hat{\sigma_N}}{V_0 \cdot a_{dist/\%}} \tag{10}$$

where $\hat{\sigma_N}$ is the calculated standard deviation of the signal over N points, V_0 is the rated voltage, and $a_{dist/\%}$ is the percentage of the amplitude variation of the disturbance.

ii) Disturbance detection condition: Using the voltage variation estimator of (10), a disturbance is detected if the condition of (11) is fulfilled.

$$\hat{E}_{dist} > l_{dist} \tag{11}$$

where l_{dist} is set between 0.2 and 0.5 in this work, regardless of the disturbance characteristics. Fig. 5 shows the comparison of the estimator $\hat{E}_{dist}$ with the limit l_{dist} during a disturbance.

② *Filtering of uncorrelated power variations*

The variation of power is measured and compared to another variation limit l_{state}, indicating a discontinuity. While the power variations are below the discontinuity limit, the load sensitivity is being calculated (see ③).

Appliances such as washing machines, dishwashers, or ovens have different working states depending on their current working cycle. Each state is recognizable by its power consumption. The power-to-voltage or power-to-frequency dependencies are also affected by the operating state (different components in use). Thus, the load sensitivity identification algorithm must be able to distinguish power fluctuations originating from the internal load behavior versus those caused by introduced disturbances. For example, a state change is considered as a power discontinuity.

i) Definition of $\hat{E}_{power}$: The power variation estimator $\hat{E}_{power}$ of (12) differentiates the case of power variations created by the voltage perturbation from the case of loads internal state changes.

$$\hat{E}_{power} = \frac{\hat{\sigma_N}}{P_{max} \cdot a_{dist/\%} \cdot n_{p_0}} \tag{12}$$

where $\hat{\sigma_N}$ is the power standard deviation calculated over N values, $a_{dist/\%}$ is the perturbation amplitude variation in percent, P_{max} is the maximum power value measured in the last time window, and n_{p_0} is the previously calculated load sensitivity. The two additional normalization parameters in comparison to (11), P_{max} and n_{p_0}, are required as they represent the current load state.

ii) Discontinuity detection condition: The condition of no discontinuity is written in (13):

$$\hat{E}_{power} < l_{state} \tag{13}$$

where l_{state} can be chosen depending on the system setups (number of loads and nominal power).

Based on the estimator value, the method can classify the power variation into different categories, namely a state change or a reaction to the perturbation in voltage or frequency.

Remarks on ① and ②: The variable N influences the value of the standard deviation $\hat{\sigma_N}$, making the detection more or less precise as shown in Fig. 5. Actually, the choice of N is influenced by the sampling rate of the measurements. We define α, representing the ratio of the number of samples in the calculation window N, to the number of samples in one period of the disturbance $N_{pt/T}$ as:

$$\alpha = \frac{N}{N_{pt/T}} \tag{14}$$

$$N_{pt/T} = \frac{T_{dist}}{t_s} \tag{15}$$

where the disturbance period $T_{dist} = 1/f_{dist} = 1.25\,\text{s}$, and the time step $t_s = 50\,\text{ms}$, in this work.

$\alpha \simeq 1$ offers a good choice for the perturbation detection, where (11) is used for the disturbance detection, regardless of the perturbation characteristics. This makes the detection criteria flexible and usable for different disturbances amplitudes and types (sinusoidal, triangular, ramp, or step). Moreover, the detection is resilient to noise, as demonstrated in Fig. 5, where the voltage is represented with a signal-to-noise ratio (SNR) of 15dB.

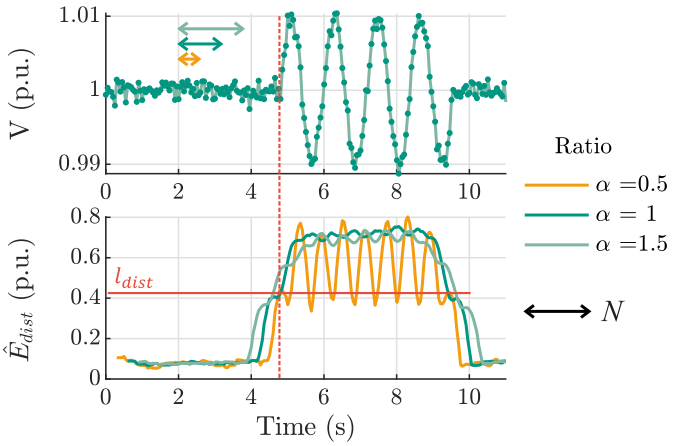

Fig. 5: Influence of the number of samples N in the calculation window (e.g. the ratio α) on the disturbance detection, with SNR=15 dB.

③ *Filtered Load Sensitivity Calculation*

Since the load sensitivity calculation is highly sensitive to measurement noise, the input signals (voltage RMS and active power, for example) must be filtered with a low-pass filter before the calculation. Then, a second filter is applied to the calculated load sensitivity values to remove eventual outliers. The data processing of the load sensitivity calculation (step ③ of Fig. 4) is detailed in Fig. 6 and explained in the following.

The voltage RMS (or frequency) and active (or reactive) power are considered as the input measurement magnitudes used for the load sensitivity calculation.

This article has been accepted for publication in IEEE Transactions on Power Delivery. This is the author's version which has not been fully edited and content may change prior to final publication. Citation information: DOI 10.1109/TPWRD.2024.3453270

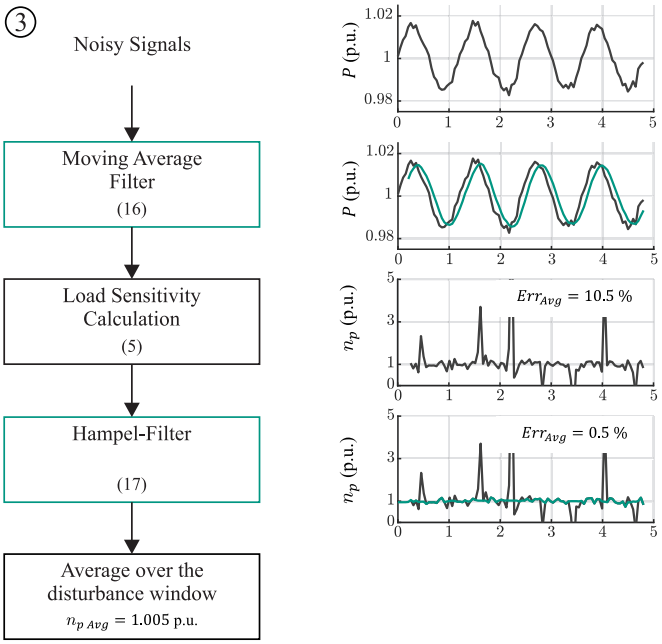

Fig. 6: Data processing for identification and result example.

i) Moving Average Filter: The moving average filter, described in (16), provides a smoothed and delayed version of the input signals and has been applied to both voltage and power signals. The window size for the average has been chosen for an optimal balance between noise reduction and signal distortion. The filter's response can be written as:

$$y(k) = \frac{1}{N} \cdot \sum_{n=1}^{N} x(k-n) \tag{16}$$

where N is the considered window size, $x(n)$ are the real measurements, and y is the new value of the signal x at the time t_k, after the application of the filter.

It must be noted that the shape of the filtered signal does not impact the load sensitivity calculation, provided the same filter parameters are used for both input signals. The filtered power signal is shown in green in Fig. 6, where the output signal has been obviously smoothed.

ii) Load Sensitivity Calculation: The load sensitivity is calculated over the disturbance window, where the detection has been explained in ① and ②. The calculation of (5) uses filtered voltage and input power. After the raw calculation, the average error of the calculation is $Err_{\text{Avg}} = 10.5\,\%$ for this showcase.

iii) Hampel-Filter: Even if the identification method uses filtered signals for the calculation of load sensitivities, some outliers are still observed, moving the final load sensitivity average away from the actual sensitivity value. Therefore, calculated load sensitivities are filtered with a Hampel-filter. This filter removes outliers by calculating the median value of the data set [52]. It considers as an outlier all points that deviate from the median more than the estimated standard deviation. The filter's response is given as:

$$y(k) = \begin{cases} m_k, & \text{if } |x(k) - m_k| > t \cdot S_k \\ x(k), & \text{otherwise} \end{cases} \tag{17}$$

where y is the filtered value of x, m_k is the median value over the moving data window, and S_k is the standard deviation estimator, using the Median Absolute Deviation (MAD), and defined as:

$$S_k = 1.4826 \cdot \text{MAD} \tag{18}$$

The factor 1.4826 makes S_k an unbiased estimator of the standard deviation for Gaussian data. The threshold parameter t is set, giving a more ($t = 0$) or less aggressive filter ($t > 0$). The filtered load sensitivity is drawn in green in Fig. 6.

iv) Average over the disturbance window: Because of the systematic sensitivity identification error described in section III-C, the calculated values are averaged over the entire perturbation window after having been filtered with the Hampel-filter. The maximum error is reduced, and the identification error after averaging falls from $Err_{\text{Avg}} = 10.5\,\%$ without filter to $Err_{\text{Avg}} = 0.5\,\%$ with the Hampel-filter, proving its effectiveness.

④ *Reliability of Calculated Load Sensitivity*

The reliability of the calculation is determined based on the two aspects described below.

i) Low surrounding noise: The load sensitivity is calculated when the power shows simultaneous variations with the voltage perturbation, which may be due to the load sensitivity. However, the power variations can be uncorrelated to the voltage disturbance, especially in cases of measurement noise or internal load behavior. In this work, the estimator of the power variation $\hat{E}_{power}$ is used as a measure of the surrounding noise. The variation of power before the disturbance $\hat{E}_{powerB}$ is compared with the variation of power during the disturbance $\hat{E}_{powerD}$. If the variation before the disturbance is bigger than the variation during it, as shown in (19), the impact of surrounding noise on the load sensitivity calculation is neglected. Otherwise, the calculated sensitivity is considered unreliable.

$$\hat{E}_{powerD} > m \cdot \hat{E}_{powerB} \tag{19}$$

where the factor m is equal to 2 in this work, and the variation estimators $\hat{E}_{powerB}$ and $\hat{E}_{powerB}$ are calculated based on (12).

ii) Small load sensitivity: Because of the remaining measurement noise, the calculation uncertainties require setting a minimum value for the load sensitivity calculation. Especially in case of no sensitivity, the algorithm is unable to differentiate very small load sensitivity (e.g. $\mid n_p \mid < 0.05$) from no sensitivity at all. Consequently, only load sensitivity greater than 0.05 is considered. This criterion will not influence further control based in the estimated sensitivity, as the controller lacks controllability on the grid power consumption in cases of excessively small load sensitivity.

iii) Average over the disturbance window After this filtering process, the load sensitivity is averaged over the disturbance window. This value is used for the voltage control described in Section II.

V. Validation of the Identification Approach in Realistic Experimental Conditions

To prove its performance, the proposed algorithm has been tested in realistic grid conditions, implementing it at the *Energy Smart Home Lab* (ESHL) at the *Karlsruhe Institute of Technology* (KIT) as in Fig. 7.

A. Energy Smart Home Lab Experimental Setup

The ESHL is a 60 m^2 intelligent residential building, with two bedrooms and a 20 m^2 technical room [53], see Fig. 7. Electrical commercial devices such as a washing machine, clothes dryer, dishwasher, coffee machine, boiler, vacuum cleaner, microwave, or oven are installed in the apartment, as described in Table II. Each phase has been measured individually, and the power measurement in one phase is equal to the power consumption of the connected loads to this phase. The house has been supplied by a three-phase four-quadrant voltage amplifier that operates as a controlled voltage source and has been connected to a real-time simulator, which provides output of the voltage signals with desired magnitude and frequency disturbances. For performing the experiments, the amplifier was tasked to apply the desired disturbance in voltage amplitude, while the frequency and active and reactive power were recorded with 20 Hz (t_s = 50 ms). The same operation has been repeated, considering frequency perturbations only.

B. Experimental Results

Figures 8a and 8b show two examples of load sensitivity calculation of a vacuum cleaner, with a frequency perturbation of $\Delta f = \pm 0.5$ Hz. The first graph shows the evaluation of the active power sensitivity to frequency n_{pf}, whereas the second one shows the calculation of n_{qf}. The raw identification is drawn in grey, whereas the green curve depicts the results obtained after filtering. Similarly, figures 9a and 9b show the power-to-voltage sensitivities calculated with measurements

TABLE II: Rated power of residential appliances, defined as the average power before the disturbance

Load	P_0 (W)	Q_0 (var)	Load	P_0 (W)	Q_0 (var)
Back oven	3450	46	Toaster	713	7
Washing machine	2150	210	Halogen light	556	115
Cloth dryer	2100	66	Vacuum cleaner	401	420
Dishwasher	2000	100	Cooker hood	214	221
Water kettle	1963	14	Freezer	108	21
Induction stove	1935	288	Fridge	41	52
Coffee machine	1000	13	Electrical shutter	123	113

of an oven, where the voltage amplitude has been varied by $\Delta V = \pm 0.5\,\%$ of the rated voltage. The first graph represents the active power sensitivity to voltage n_{pv}, while the second one depicts the reactive power measurements, giving n_{qv}.

1) Example of the calculation implementation for real loads: The algorithm computes the load sensitivity exclusively during detected disturbances. As depicted in figures 8a and 8b, and figures 9a and 9b, the sensitivity calculation window perfectly aligns with the disturbance window, showcasing the effectiveness of the detection method in distinguishing between baseline measurements and disturbances. In the third graph representing the load sensitivity, the grey curve represents the raw calculation, while the green curve shows the filtered load sensitivity using the Hampel-filter. The single point separated from the calculation window represents the average of the filtered calculation. Figures 8a and 8b show the results of three independent calculations of the vacuum cleaner load sensitivity to frequency: $n_{pf} = -1.89$ and $n_{qf} = -0.49$.

Similarly, figures 9a and 9b show the calculation of the load sensitivity to voltage of an oven, despite the state change (at $t \simeq 20$ s). The first graph depicts a step in the oven's active power, occurring during the perturbation generated for the load sensitivity calculation. After the filtering stage, the algorithm still gives a reliable value, as the load sensitivity average of the

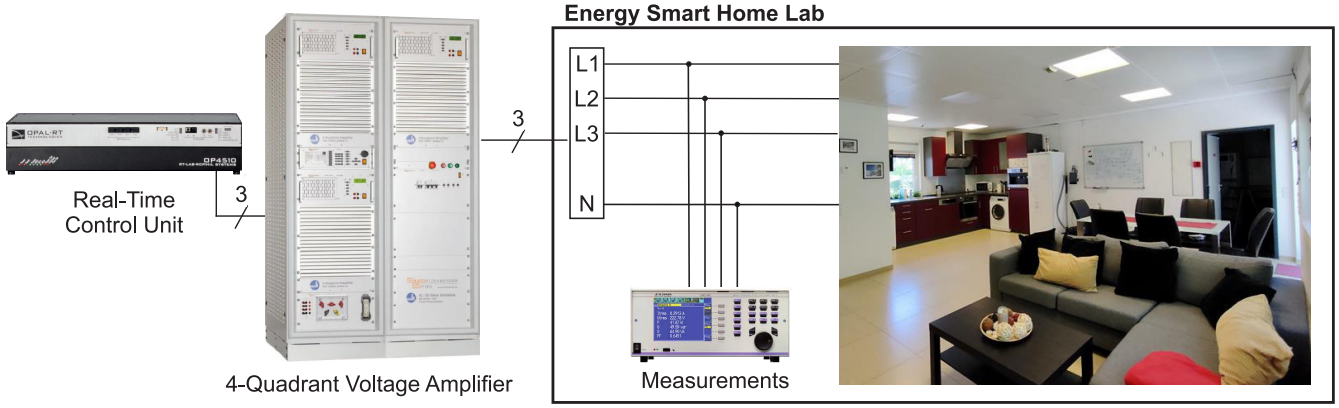

Fig. 7: Set-ups for real measurements in the Energy Smart Home Lab

second voltage perturbation is identical to both the previous and the following one. The oven's active power sensitivity to voltage identification gave $n_{pv} = 2.00$. The second graph shows the reactive power peak due to the active power sudden change. The power discontinuity detection recognizes that this high power variation does not come from the created voltage disturbance and stops the load sensitivity identification. The oven's reactive power sensitivity to voltage has been accurately evaluated: $n_{qv} = 3.05$.

The algorithm is thus able to perform the load sensitivity calculation with realistic household load behaviors and can reject unwanted power variations, avoiding identification errors.

2) Validation of the load parameter identification by means of power reconstruction: Working with real loads, the actual load sensitivity is unknown. The comparison of the measured power and the reconstructed power provides information on the calculation's reliability.

First, the load sensitivity calculation is consistent, giving the same results for all independently made calculations. Then, the measured oven's powers of figures 9a and 9b have been compared to a reconstructed power based on the exponential load model and the calculated load sensitivity of the oven. Fig. 10 provides this comparison, where the reconstructed power is shown in green, and the measured power is plotted in grey.

During power variations, the reconstructed power magnitude matches the measured power magnitude of the disturbance. Indeed, the relative error of the reconstructed power to the measurements is smaller than 0.15 %. Since the actual load sensitivity is unknown, the calculated value is varied by ± 0.1 to assess the accuracy of the estimated sensitivity. The results shown in Fig. 11 highlight that the reconstruction error

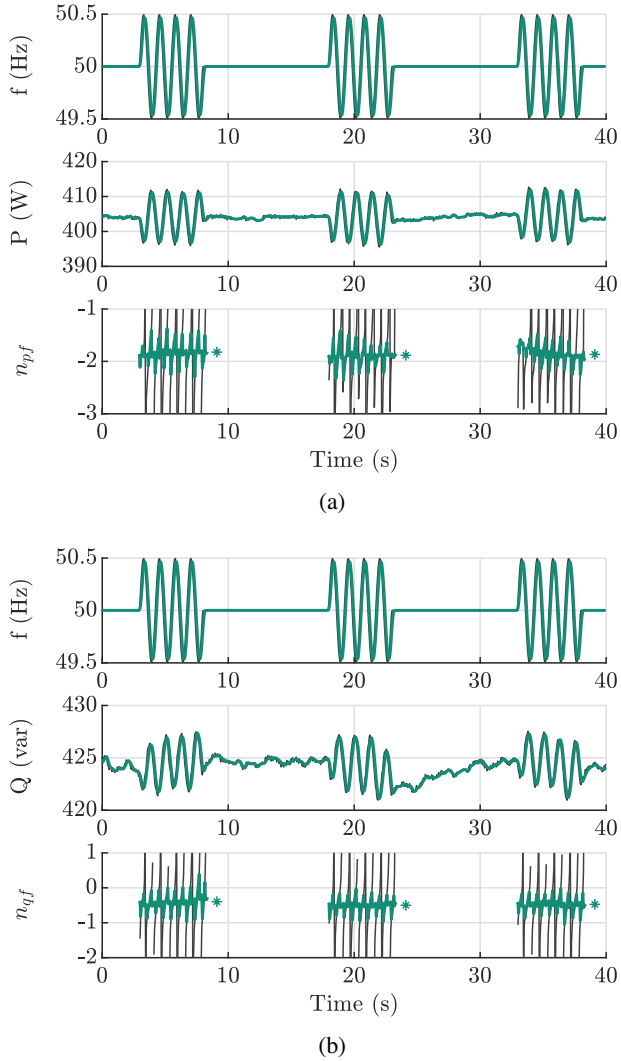

Fig. 8: Vacuum cleaner active (a) and reactive (b) power sensitivities to frequency for 1 % frequency disturbance: $n_{pf} = -1.89$ and $n_{qf} = -0.49$. For n_{pf} and n_{qf}, the raw calculation is represented in grey and the filtered values in green.

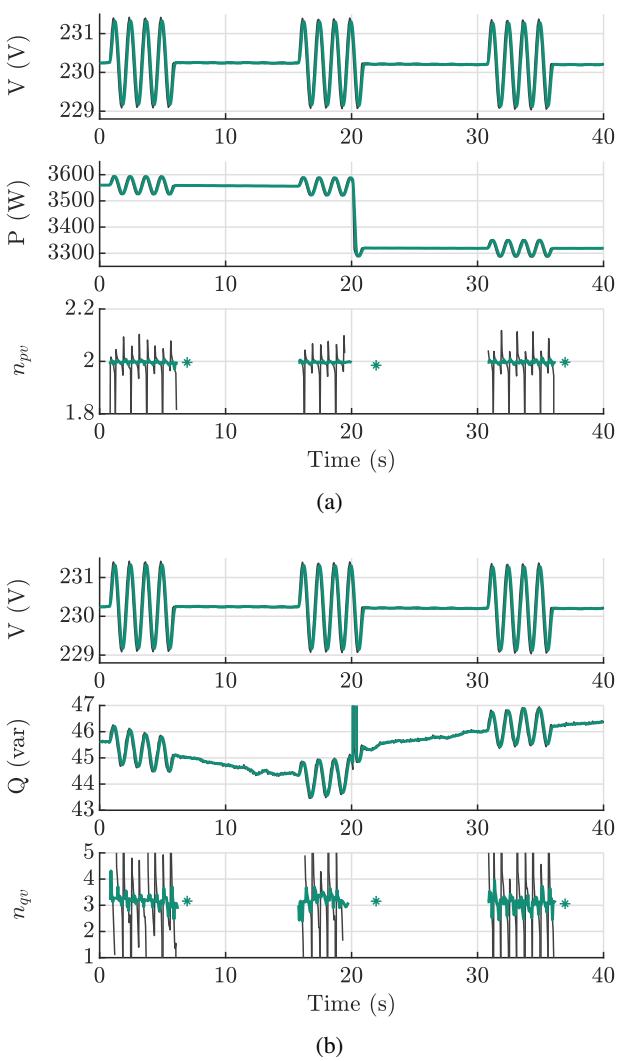

Fig. 9: Oven active (a) and reactive (b) power sensitivities to voltage for 0.5 % voltage disturbance: $n_{pv} = 2.00$ and $n_{qv} = 3.05$. For n_{pv} and n_{qv}, the raw calculation is represented in grey and the filtered values in green.

increases when the load sensitivity deviates from the estimated value $n_{pv\cdot Avg} = 2.00$, indicating that the sensitivity has been calculated with an accuracy better than 0.1. Thus, the proposed identification approach is resilient to unwanted disturbances and accurately identifies the load dependency on voltage and frequency.

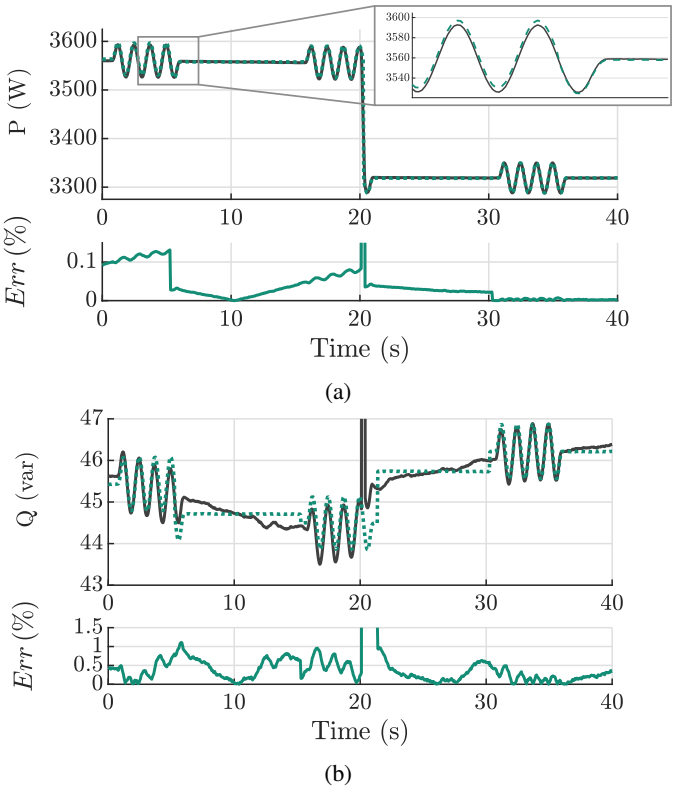

Fig. 10: Oven active (a) and reactive (b) power reconstruction for 0.5 % voltage disturbance, showing the initial power measurements in grey, and the reconstructed power using the load sensitivity identification algorithm in green.

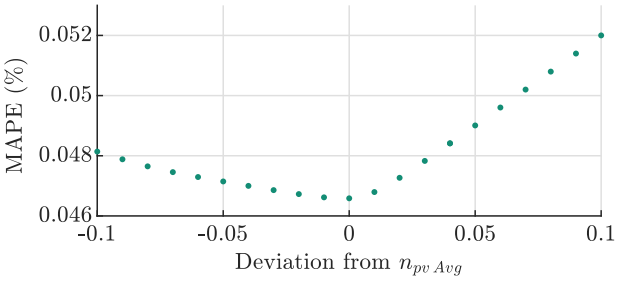

Fig. 11: Mean average percentage error (MAPE) of the reconstructed power of the oven, for the calculated load sensitivity $n_{pv\cdot Avg} = 2.00$ and deviations of ± 0.1 (see Fig. 9a and 10a).

3) Summary of the results:

- The load sensitivity is calculated only during disturbances, demonstrating the method's ability to distinguish disturbances from baseline measurements.
- The method effectively differentiates between disturbances caused by on-demand voltage (or frequency) variations and those due to measurement noise or load state changes.
- Despite internal load behavior or measurement noise, the calculated load sensitivity remains reliable, with consistent values and accurate power reconstruction.

VI. Conclusion

This paper proposes a perturbation-based load sensitivity calculation method, suitable for realistic household scenarios, using a variation-based perturbation detection algorithm. The algorithm accurately identify the load sensitivity within the range $[-5; 10]$. It detects frequency or voltage disturbances within $\Delta f \in [\pm 0.1\,\text{Hz}; \pm 1\,\text{Hz}]$ and $\Delta V \in [\pm 1\,\%; \pm 5\,\%]$ of V_0, distinguishing them in real-time from baseline measurements. The disturbance detection has been successfully applied to noisy measurements, making it suitable for on-field applications. The computational autonomy and management of uncorrelated power variations ensure consistent and reliable load sensitivity calculations. The accuracy has been demonstrated by reconstructing the measured power using the calculated load sensitivity with less than 2 % error.

References

[1] E. Sarker, P. Halder, M. Seyedmahmoudian, E. Jamei, B. Horan, S. Mekhilef, and A. Stojcevski, "Progress on the demand side management in smart grid and optimization approaches," *International Journal of Energy Research*, vol. 45, no. 1, p. 36–64, 2020.

[2] G. Strbac, "Demand side management: Benefits and challenges," *Energy Policy*, vol. 36, no. 12, pp. 4419–4426, 2008, foresight Sustainable Energy Management and the Built Environment Project. [Online]. Available: https://www.sciencedirect.com/science/article/pii/S0301421508004606

[3] Y. Gong, Y. Cai, Y. Guo, and Y. Fang, "A privacy-preserving scheme for incentive-based demand response in the smart grid," *IEEE Transactions on Smart Grid*, vol. 7, no. 3, pp. 1304–1313, 2016.

[4] A. Paverd, A. Martin, and I. Brown, "Security and privacy in smart grid demand response systems," in *Smart Grid Security*, J. Cuellar, Ed. Cham: Springer International Publishing, 2014, pp. 1–15.

[5] Y. Yan, Y. Qian, H. Sharif, and D. Tipper, "A survey on smart grid communication infrastructures: Motivations, requirements and challenges," *IEEE Communications Surveys and Tutorials*, vol. 15, no. 1, pp. 5–20, 2013.

[6] M. Diaz-Aguiló, J. Sandraz, R. Macwan, F. de León, D. Czarkowski, C. Comack, and D. Wang, "Field-validated load model for the analysis of cvr in distribution secondary networks: Energy conservation," *IEEE Transactions on Power Delivery*, vol. 28, no. 4, pp. 2428–2436, 2013.

[7] Z. Wang and J. Wang, "Review on implementation and assessment of conservation voltage reduction," *IEEE Transactions on Power Systems*, vol. 29, no. 3, pp. 1306–1315, 2014.

[8] M. S. Hossan and B. Chowdhury, "Comparison of time-varying load models for estimating cvr factor and vsf using dual-stage adaptive filter," *IEEE Transactions on Power Delivery*, vol. 34, no. 3, pp. 1001–1010, 2019.

[9] M. Liserre, G. Buticchi, M. Andresen, G. De Carne, L. F. Costa, and Z.-X. Zou, "The smart transformer: Impact on the electric grid and technology challenges," *IEEE Industrial Electronics Magazine*, vol. 10, no. 2, pp. 46–58, 2016.

[10] G. De Carne, G. Buticchi, M. Liserre, and C. Vournas, "Load control using sensitivity identification by means of smart transformer," *IEEE Transactions on Smart Grid*, vol. 9, no. 4, pp. 2606–2615, 2018.

[11] A. Ballanti and L. F. Ochoa, "Voltage-led load management in whole distribution networks," *IEEE Transactions on Power Systems*, vol. 33, no. 2, pp. 1544–1554, 2018.

[12] A. Ballanti, L. N. Ochoa, K. Bailey, and S. Cox, "Unlocking new sources of flexibility: Class: The world's largest voltage-led load-management project," *IEEE Power and Energy Magazine*, vol. 15, no. 3, pp. 52–63, 2017.

[13] A. Bokhari, A. Alkan, R. Dogan, M. Diaz-Aguiló, F. de León, D. Czarkowski, Z. Zabar, L. Birenbaum, A. Noel, and R. E. Uosef, "Experimental determination of the zip coefficients for modern residential, commercial, and industrial loads," *IEEE Transactions on Power Delivery*, vol. 29, no. 3, pp. 1372–1381, 2014.

[14] J. V. Milanovic, K. Yamashita, S. Martinez Villanueva, S. Z. Djokic, and L. M. Korunović, "International industry practice on power system load modeling," *IEEE Transactions on Power Systems*, vol. 28, no. 3, pp. 3038–3046, 2013.

[15] K. J. Leinakse M, "Exponential to zip and zip to exponential load model conversion: Methods and error." *IET Gener TransmDistrib.*, vol. 15, p. 177–193, 2021.

[16] A. Tavlintsev, A. Pankratov, and I. Lipnitskiy, "Classification of measurement-based approaches to load model identification," *Przeglad Elektrotechniczny*, vol. 97, no. 1, pp. 64–68, 2020.

[17] "Ieee guide for load modeling and simulations for power systems," *IEEE Std 2781-2022*, pp. 1–88, 2022.

[18] S. A. Arefifar and W. Xu, "Online tracking of voltage-dependent load parameters using ultc created disturbances," *IEEE Transactions on Power Systems*, vol. 28, no. 1, pp. 130–139, 2013.

[19] J. Xu, B. Xie, S. Liao, D. Ke, Y. Sun, X. Jiang, and J. Yu, "Cvr based real-time power fluctuation smoothing control for distribution systems with high penetration of pv and experimental demonstration," *IEEE Transactions on Smart Grid*, pp. 1–1, 2022.

[20] G. De Carne, M. Liserre, and C. Vournas, "On-line load sensitivity identification in lv distribution grids," *IEEE Transactions on Power Systems*, vol. 32, no. 2, pp. 1570–1571, 2017.

[21] G. De Carne, S. Bruno, M. Liserre, and M. La Scala, "Distributed online load sensitivity identification by smart transformer and industrial metering," *IEEE Transactions on Industry Applications*, vol. 55, no. 6, pp. 7328–7337, 2019.

[22] S. M. H. Rizvi, K. S. Sajan, and A. K. Srivastava, "Synchrophasor based zip parameters tracking using ml with adaptive window and data anomalies," *IEEE Transactions on Power Systems*, vol. 37, no. 1, pp. 3–13, 2022.

[23] Z. Ma, Y. Xiang, and Z. Wang, "Robust conservation voltage reduction evaluation using soft constrained gradient analysis," *IEEE Transactions on Power Systems*, pp. 1–1, 2022.

[24] Tushar, S. Pandey, A. K. Srivastava, P. Markham, N. Bhatt, and M. Patel, "Data-driven parameter estimation of steady-state load models," in *2016 IEEE International Conference on Power Electronics, Drives and Energy Systems (PEDES)*, 2016, pp. 1–5.

[25] Tushar, S. Pandey, A. K. Srivastava, P. Markham, and M. Patel, "Online estimation of steady-state load models considering data anomalies," *IEEE Transactions on Industry Applications*, vol. 54, no. 1, pp. 712–721, 2018.

[26] Z. Wang and J. Wang, "Time-varying stochastic assessment of conservation voltage reduction based on load modeling," *IEEE Transactions on Power Systems*, vol. 29, no. 5, pp. 2321–2328, 2014.

[27] J. Zhao, Z. Wang, and J. Wang, "Robust time-varying load modeling for conservation voltage reduction assessment," *IEEE Transactions on Smart Grid*, vol. 9, no. 4, pp. 3304–3312, 2018.

[28] M. Leinakse and J. Kilter, "Processing and filtering digital fault recorder events for load model estimation," in *2021 IEEE PES Innovative Smart Grid Technologies Europe (ISGT Europe)*, 2021, pp. 01–05.

[29] M. Kabiri and N. Amjady, "A hybrid estimation and identification method for online calculation of voltage-dependent load parameters," *IEEE Systems Journal*, vol. 13, no. 1, pp. 792–801, 2019.

[30] C. A. Baone, S. Veda, Y. Pan, W. Premerlani, J. Dai, and A. Johnson, "Measurement based static load model identification," in *2015 IEEE Power and Energy Society General Meeting*, 2015, pp. 1–5.

[31] X. Tang, K. N. Hasan, J. V. Milanović, K. Bailey, and S. J. Stott, "Estimation and validation of characteristic load profile through smart grid trials in a medium voltage distribution network," *IEEE Transactions on Power Systems*, vol. 33, no. 2, pp. 1848–1859, 2018.

[32] Y. Zhu and J. V. Milanović, "Automatic identification of power system load models based on field measurements," *IEEE Transactions on Power Systems*, vol. 33, no. 3, pp. 3162–3171, 2018.

[33] M. Leinakse, P. Tani, and J. Kilter, "Impact of distributed generation on estimation of exponential load models," in *2019 IEEE Power Energy Society General Meeting (PESGM)*, 2019, pp. 1–5.

[34] M. Leinakse, G. Andreesen, P. Tani, and J. Kilter, "Estimation of exponential and zip load model of aggregated load with distributed generation," in *2021 IEEE 62nd International Scientific Conference on Power and Electrical Engineering of Riga Technical University (RTUCON)*, 2021, pp. 1–6.

[35] M. Courcelle, Q. Tao, J. Geis-Schroer, S. Bruno, T. Leibfried, and G. De Carne, "Methods comparison for load sensitivity identification," in *2023 IEEE Belgrade PowerTech*, 2023, pp. 1–6.

[36] J. Wang, A. Raza, T. Hong, A. C. Sullberg, F. de León, and Q. Huang, "Analysis of energy savings of cvr including refrigeration loads in distribution systems," *IEEE Transactions on Power Delivery*, vol. 33, no. 1, pp. 158–168, 2018.

[37] M. Liserre, G. Buticchi, M. Andresen, G. De Carne, L. F. Costa, and Z.-X. Zou, "The smart transformer: Impact on the electric grid and technology challenges," *IEEE Industrial Electronics Magazine*, vol. 10, no. 2, pp. 46–58, 2016.

[38] L. Ferreira Costa, G. De Carne, G. Buticchi, and M. Liserre, "The smart transformer: A solid-state transformer tailored to provide ancillary services to the distribution grid," *IEEE Power Electronics Magazine*, vol. 4, no. 2, pp. 56–67, 2017.

[39] K. Mainali, A. Tripathi, S. Madhusoodhanan, A. Kadavelugu, D. Patel, S. Hazra, K. Hatua, and S. Bhattacharya, "A transformerless intelligent power substation: A three-phase sst enabled by a 15-kv sic igbt," *IEEE Power Electronics Magazine*, vol. 2, no. 3, pp. 31–43, 2015.

[40] H. Chen and D. Divan, "Design of a 10-kv·a soft-switching solid-state transformer (s4t)," *IEEE Transactions on Power Electronics*, vol. 33, no. 7, pp. 5724–5738, 2018.

[41] S. Giacomuzzi, M. Langwasser, G. De Carne, G. Buja, and M. Liserre, "Smart transformer-based medium voltage grid support by means of active power control," *CES Transactions on Electrical Machines and Systems*, vol. 4, no. 4, pp. 285–294, 2020.

[42] S. Giacomuzzi, G. Buja, G. D. Carne, and M. Liserre, "Application of smart transformer load control to mitigate voltage fluctuations in medium voltage networks," in *2018 IEEE Power Energy Society General Meeting (PESGM)*, 2018, pp. 1–5.

[43] Q. Tao, J. Geis-Schroer, F. Wald, M. Courcelle, M. Langwasser, T. Leibfried, M. Liserre, and G. De Carne, "The potential of frequency-based power control in distribution grids," in *2022 IEEE 13th International Symposium on Power Electronics for Distributed Generation Systems (PEDG)*, 2022, pp. 1–6.

[44] F. Wald, Q. Tao, and G. D. Carne, "Virtual synchronous machine control for asynchronous grid connections," *IEEE Transactions on Power Delivery*, pp. 1–10, 2023.

[45] L. Ferreira Costa, G. De Carne, G. Buticchi, and M. Liserre, "The smart transformer: A solid-state transformer tailored to provide ancillary services to the distribution grid," *IEEE Power Electronics Magazine*, vol. 4, no. 2, pp. 56–67, 2017.

[46] M. Langwasser, G. De Carne, M. Liserre, and M. Biskoping, "Voltage-based load control for frequency support provision by hvdc systems," in *IECON 2018 - 44th Annual Conference of the IEEE Industrial Electronics Society*, 2018, pp. 311–316.

[47] M. L. M. Langwasser, G. D. Carne and M. Biskoping, "Enhanced grid frequency support by means of hvdc-based load control," no. 189, p. 106552, 2020.

[48] X. Gao, G. De Carne, M. Langwasser, and M. Liserre, "Online load control in medium voltage grid by means of reactive power modification of fast charging station," in *2019 IEEE Milan PowerTech*, 2019, pp. 1–6.

[49] X. Gao, G. De Carne, M. Andresen, S. Brüske, S. Pugliese, and M. Liserre, "Voltage-dependent load-leveling approach by means of electric vehicle fast charging stations," *IEEE Transactions on Transportation Electrification*, vol. 7, no. 3, pp. 1099–1111, 2021.

[50] J. V. Milanović, "On unreliability of exponential load models," *Electric Power Systems Research*, vol. 49, no. 1, pp. 1–9, 1999. [Online]. Available: https://www.sciencedirect.com/science/article/pii/S0378779698000479

[51] L. M. Korunovic, J. V. Milanovic, S. Z. Djokic, K. Yamashita, S. M. Villanueva, and S. Sterpu, "Recommended parameter values and ranges of most frequently used static load models," *IEEE Transactions on Power Systems*, vol. 33, no. 6, pp. 5923–5934, 2018.

[52] R. Pearson, "Outliers in process modeling and identification," *IEEE Transactions on Control Systems Technology*, vol. 10, no. 1, pp. 55–63, 2002.

[53] S. Kochanneck, I. Mauser, B. Bohnet, S. Hubschneider, H. Schmeck, M. Braun, and T. Leibfried, "Establishing a hardware-in-the-loop research environment with a hybrid energy storage system," in *2016 IEEE Innovative Smart Grid Technologies - Asia (ISGT-Asia)*, 2016, pp. 497–503.

This article has been accepted for publication in IEEE Transactions on Power Delivery. This is the author's version which has not been fully edited and content may change prior to final publication. Citation information: DOI 10.1109/TPWRD.2024.3453270

Maëva Courcelle (S'22) received her M.Sc. degree equivalent (Diplôme d'Ingénieur) from Telecom Physique Strasbourg, Illkirch-Graffenstaden, France, in 2021. During her general engineering studies majoring in electronics and embedded systems, she deepened her knowledge in power electronics as an exchange student at the Karlsruhe Institute of Technology (KIT), Karlsruhe, Germany. Since the end of 2021, she has been pursuing a Ph.D. degree as part of the "Real-Time Systems for Energy Technologies" Group and the "Energy Lab" at KIT. In 2024, she spent one semester as a visiting researcher at the FREEDM Systems Center at North Carolina State University, USA. Her research interests include real-time load parameter identification for the modeling and control of distribution networks.

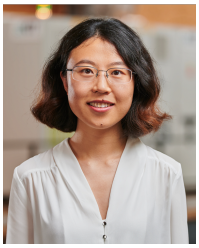

Qiucen Tao (S'22) received her B.Sc. degree from Southeast University, China, in 2017, and her M.Sc. degree from the Karlsruhe Institute of Technology (KIT), Karlsruhe, Germany, in 2021, both in electrical engineering. She is currently pursuing her Ph.D. degree as a member of the "Real-Time Systems for Energy Technologies" Group and the "Energy Lab" at KIT. Her research interests include load sensitivity identification, demand-side management, smart distribution networks, and the real-time simulation and power hardware-in-the-loop implementation of these systems.

Johanna Geis-Schroer (S'23) received her B.Sc. degree in industrial engineering in 2017, and her M.Sc. degree in electrical engineering in 2020, both from the Karlsruhe Institute of Technology (KIT), Karlsruhe, Germany. In 2019, she spent one semester as a research intern at the Energy Production and Infrastructure Center at the University of North Carolina at Charlotte, North Carolina, USA. Currently, she is pursuing her Ph.D. degree in electrical engineering at KIT, and is working as a research associate at the Institute of Electric Energy Systems and High-Voltage Technology (IEH) at KIT. Her research interests include frequency dynamics in low-inertia power systems, load modeling, and the impacts of large frequency variations on loads and grid equipment.

Thomas Leibfried (M' 96, SM' 20) received the Dipl.-Ing. and Dr.-Ing. degrees in electrical engineering from the University of Stuttgart, Stuttgart, Germany, in 1990 and 1996, respectively. From 1996 to 2002, he was with Siemens AG, Nuremberg, Germany, working in the power transformer business in various technical and management positions. In 2002, he joined the University of Karlsruhe (now Karlsruhe Institute of Technology, KIT), Karlsruhe, Germany, as the head of the Institute of Electric Energy Systems and High-Voltage Technology (IEH). From 2014 to 2018 he served as Dean of his faculty. In 2024, he was elected as member of the scientific council "Electrical Engineering and Information Technology" within the German research foundation for the period 2024-2028. His research interests are power electronic applications in the power grid, stability of grids with high power electronic penetration and high-voltage technology. He is a member of VDE and CIGRE.

Giovanni De Carne (S'14, M'17, SM'21) received the B.Sc. and M.Sc. degrees in electrical Engineering from the Polytechnic University of Bari, Italy, in 2011 and 2013, respectively, and the Ph.D. degree from the Chair of Power Electronics, Kiel University, Germany, in 2018. Prof. De Carne is currently W3 (full) professor at the Institute for Technical Physics at the Karlsruhe Institute of Technology, Karlsruhe, Germany, where he leads the "Real-Time Systems for Energy Technologies" Group and the "Power Hardware In the Loop Lab". He is currently supervising PhD students, managing academic and industrial projects, and developing multi-MW power hardware in the loop testing infrastructures for energy storage systems and hydrogen-based drives. He has authored/coauthored more than 100 peer-reviewed scientific papers. His research interests include power electronics integration in power systems, solid state transformers, real time modelling, and power hardware in the loop. Prof. De Carne successfully hosted the IEEE eGrid2023 Workshop in Karlsruhe in October 2023 with high participation from industry. He has been technical program committee chair for several IEEE conferences, associate editor of the IEEE Open Journal of Power Electronics and several other IEEE and IET journals.